An *Ab Initio* Approach Towards Engineering Fischer-Tropsch Surface Chemistry

Type of Report: Final Technical Report

Report Period: 9/11/2001- 9/11/2006

Principle Author: Matthew Neurock

Date: January 30, 2007

DOE Award Number: DE-FG26-01NT41275

Name and Address of Submitting Organization:

Professor Matthew Neurock
Department of Chemical Engineering
102 Engineers' Way
University of Virginia
Charlottesville, VA 22904-4741

DISCLAIMER

I. ABSTRACT

One of the greatest societal challenges over the next decade is the production of cheap, renewable energy for the 10 billion people that inhabit the earth. This will require the development of various energy sources which will likely include fuels derived from methane, coal, and biomass and alternatives sources such as solar, wind and nuclear energy. One approach will be to synthesize gasoline and other fuels from simpler hydrocarbons such as CO derived from methane or other U.S. based sources such as coal. Syngas (CO and H_2) can be readily converted into higher molecular weight hydrocarbons through Fischer-Tropsch synthesis. Fischer-Trosch (FT) synthesis involves the adsorption and the activation of CO and H_2, the subsequent propagation steps including hydrogenation and carbon-carbon coupling, followed by chain termination reactions. The current commercial catalysts are supported Co and Co-alloys particles. This project set out with the following objectives in mind: *1) understand the reaction mechanisms that control FT kinetics, 2) predict how the intrinsic metal-adsorbate bond affects the sequence of elementary steps in FT, 3) establish the effects of the reaction environment on catalytic activity and selectivity, 4) construct a first-principles based algorithm that can incorporate the detailed atomic surface structure and simulate the kinetics for the myriad of elementary pathways that make up FT chemistry, and 5) suggest a set of optimal features such as alloy composition and spatial configuration, oxide support, distribution of defect sites. As part of this effort we devoted a significant portion of time to develop an ab initio based kinetic Monte Carlo simulation which can be used to follow FT surface chemistry over different transition metal and alloy surfaces defined by the user.* Over the life of this program, we have used theory and have developed and applied stochastic Monte Carlo simulations in order to establish the fundamental catalytic processes that control FT synthesis, thus enabling us to accomplish the first 4 of these objectives. In addition, we were able to begin to suggest the design features of these materials, the final task of the proposed effort. The following report details the specific findings and proposes recommendations. The support from DOE NETL was used to fund a portion of a postdoctoral and a graduate student's salaries. The postdoctoral fellow (Dr. Qingfeng Ge) who was working on this project was hired as an Assistant Professor in chemistry at the Southern Illinois University.

II. TABLE OF CONTENTS

III. INTRODUCTION

Fischer-Tropsch synthesis involves the conversion of syngas, CO and H_2, to long-chain hydrocarbons for the production of gasoline, fuel or heating oil. The reaction is currently practiced by Sasol in the South Africa to produce diesel from syngas produced from natural gas and coal feedstock. Similarly, the Shell Oil Company uses the Fischer-Tropsch reaction to produce 14,700 bbl/day of higher molecular weight products from natural gas syngas. Fischer-Tropsch synthesis produces very high purity hydrocarbons that can be used as fuels and feedstock for other petrochemical processes, depending on the molecular weight range that is distilled. The products are virtually free of sulfur, nitrogen and metallic contaminants, which makes them environmentally friendly. In the more than 80 years since Fischer and Tropsch discovered this process, a large number of studies have been conducted to elucidate the mechanism and to determine the optimum operating conditions to maximize the desired products.[4-23] Most of these studies have focused on the synthesis and characterization of different catalysts. While these studies are essential for catalyst development and industrial reactor design, there is still a very strong need to understand the mechanisms which control the Fischer-Tropsch reaction at a molecular level in order to be able to design catalysts that can more precisely control the selectivity, improve the activity and enhance catalysts lifetimes.

Elementary Steps In Fischer Tropsch Synthesis

Fischer-Tropsch synthesis is comprised of a complex network of elementary bond-breaking and bond-forming steps which includes CO and H_2 activation, hydrogenation and hydrocarbon chain growth over supported metal particles. Currently the best FT catalysts lie in the middle of the periodic table as they provide an optimal degree of bond-breaking and bond-making functionality. Metallic Co and Fe are the two metals that have shown the most promise. Cobalt readily dissociates CO and subsequently carries out hydrogenation and hydrocarbon coupling without one dominating over the other, thus leading to longer hydrocarbon chain product. Transition metals to the left of Co in the periodic table readily activate CO but the adsorbed C and O intermediates that form are too strongly bound to the surface. The C atoms that form tends to lead to carbide that hinders subsequent hydrogenation and coupling reactions [24-26]. Iron, which is just to the left of Co, readily activates CO but has a strong tendency to form surface carbides that are typically less active than Co**.[25]** As one moves the right in the periodic table, bond-making is enhanced at the expense of bond-breaking functionality. Nickel, which lies just to the right of Co, is less active in dissociating CO than Co but facilitates more rapid hydrogenation, thus leading to the preferential formation of methane [24, 25]. As one moves further to the right it becomes difficult to activate the CO bond, and CO hydrogenation becomes the preferred path. This is consistent with the fact that methanol synthesis is typically carried out of supported Cu and Pd along with the presence of a promoter [24, 25]. The most active FT catalysts appear to be Ru-promoted Co[7, 8, 21] and base-promoted iron which balance the necessary elementary steps.

Despite the significant research efforts and progress in FT and oxygenate synthesis, the fundamental understanding of the how the atomic surface structure of the catalyst controls

the elementary molecular transformations is still not well-understood. The complexity of the chemistry in these systems has made it difficult to readily discover new catalytic materials and optimal operating conditions. A more complete understanding of the fundamental processes that control the overall catalytic performance would therefore be quite valuable. Herein we provide a detailed report on a comprehensive set of elementary steps important for both FT over model Co surfaces and some CoRu alloys. This includes CO activation, CH_x hydrogenation, C-C coupling, water formation, and CO hydrogenation.

IV. EXECUTIVE SUMMARY

Concerns over the dwindling oil supply and energy independence have fueled a strong resurgence in Fischer-Tropsch synthesis as an alternative source of liquid hydrocarbon fuels from sources such as methane and coal. Fischer-Tropsch synthesis involves a complex set of bond breaking and bond making reactions which lead to synthesis of longer hydrocarbons that can be used to produce a range of different fuel, heating oil as well as petrochemical intermediates. The delicate balance between the different elementary steps dictates the ultimate product distribution. The elementary steps include the adsorption and subsequent activation of CO and H_2, the hydrogenation of hydrocarbon surface intermediates, the coupling of hydrocarbon intermediates, the termination of growing hydrocarbon chains and the desorption of products. The step which appears to dictate the rate involves the activation of CO. The selectivity to a particular product slate is ultimately controlled by a competing balance between the hydrogenation and hydrocarbon coupling kinetics. While FT synthesis has been studied for many years, there is still a rather poor fundamental understanding of the intrinsic kinetics for the elementary CO dissociation, CH_x hydrogenation, CH_x coupling reactions, surface diffusion reactions or the surface coverages. As such there is little understanding of how the atomic surface structure influences catalytic performance. In an effort to examine this system in detail, we have carried out ab initio quantum mechanical calculations to determine the kinetics for elementary steps and kinetic Monte Carlo simulation to track the changes in the surface and product distribution to changes in the surface structure as well as changes in the operating conditions.

Density functional theoretical calculations were carried out to determine the binding energies for CO, CH_x, C_2H_x, CH_xO_y, $C_2H_xO_y$, H_2O, as well as the smaller (O, H, OH, C, etc.) intermediates over the model Co(0001), corrugated Co$\{11\bar{2}0\}$, and stepped Co$\{10\bar{1}2\}$ and $\{11\bar{2}4\}$ surfaces. In addition, we calculated the overall reaction energies as well as the activation barriers associated with CO activation, CH_x hydrogenation, CH_x coupling, and CHO hydrogenation in order to elucidate the fundamental chemistry and establish a more comprehensive database for these reactions. The database was ultimately used in the stochastic kinetic simulations. The results indicate that CO activation likely occurs over the stepped or defect sites on the surface.[3] The barriers tend to be on the order of 100 kJ/mol more favorable for CO to activate at the stepped sites than on the Co(0001) terraces. [3] The local surface coverage can also dictate the relative difficulty of activating the CO bond. At higher, more realistic surface coverages, it is much more difficult to activate CO. The addition of Ru to the Co surface appeared to significantly enhance this reaction.[7, 8, 21] The subsequent hydrogenation and hydrocarbon coupling reactions were found to have similar activation barriers. This suggests that there is an optimal balance between the hydrogenation and hydrocarbon coupling surface reactions that leads to higher selectivities over Co. Metals which are near the center of the periodic table tend to promote hydrogenation which leads to methane production. [25] For metals that lie to the far right, the CO bond does not activate and one instead promotes methanol formation rather than hydrocarbons. Metals to the left in the period table readily dissociate CO and lead to result in a stronger adherence of carbon on the surface. [25] This however acts to promote coke or graphite

formation, and in addition, the formation of a carbide layer which can then produce a surface carbide.

An ab initio based kinetic Monte Carlo code was developed and applied as part of this project which we ultimately used to follow the molecular transformations over the surface. The KMC algorithm allows the user the ability to change the local surface structure, alloy a second metal, and change the local atomic arrangements of the two metals. This allows one to use the code to screen the influence of changes in the process parameters and/or atomic surface structure and composition.

In addition, the KMC simulations begin to provide a link between the idealized theoretical calculations which are typically carried out at low surface coverage conditions and 0 K and more realistic operating conditions by embedding models that describe the nature of lateral interactions between coadsorbed molecules that take place at higher coverages and are the result of more realistic higher pressures conditions. The simulations can thus be used to carry out "virtual experiments" to probe the sensitivity of different reactions and or kinetics to the resulting catalytic performance. In addition, they can be used to provide insight into the relative importance of different reaction pathways. This can be performed by turning on and off specific reactions or adjusting their calculated rate constants. This also provides insight into the governing reaction mechanisms.

The simulation results show that the chemistry requires that CO activate at defect sites. The surface appears to be predominantly covered by CO. The largest CH_x* surface intermediate is CH* which is present at about 10%. The barriers for hydrogenation as well as hydrocarbon coupling both appear to be favored on the terrace sites. The coupling most favorably proceeds via CH* + CH_2* although we can not rule out CH* + CO* as a potential pathway just yet. We have shown that both Cu as well as Pd tend to leave the CO bond intact and offer lower barriers for hydrogenation which indicates that they would be best for methanol synthesis. This is consistent with experimental results. In addition, the simulations suggest that surface alloys comprised of Sn into surface Pt(111) helps to substantially promotes this reaction. In addition, Au/Cd(0001) also appears to be quite interesting. These ideas need to be examined further with experimental in order to see if one can achieve this behavior.

V. COMPUTATIONAL METHODS

Ab Initio Quantum Mechanical Calculations

Ab initio quantum mechanical calculations were carried out in order to determine the optimal adsorption sites and the corresponding adsorption energies for the intermediates examined, the overall reaction energies for a range of different surface reactions and the activation barriers for each of these reactions. More specifically we used periodic density functional theoretical calculations as implemented in Vienna ab initio simulation program (VASP) [27, 28]. All of the calculations were performed using plane waves basis functions with a cut off energy of 320 eV and ultrasoft pseudopotentials to describe electron-ion interactions[29]. The PW91 form of generalized gradient approximation was used to describe exchange and correlation energies[30]. All of the calculations were carried out using spin polarization since cobalt is ferromagnetic in nature. Convergence tests for cutoff energy were carried out with an increased cutoff energy of 400 eV which showed a change in the energy of only 0.1 eV.

The calculations on the Co(0001) surface was carried out at various different unit cell sizes ultimately to test coverage effects. The slab thicknesses for all of the Co(0001) calculations was fixed at 4 metal layers with over 12 angstroms of vacuum between the slabs. A 3x3x1 k-point mesh was used to sample the first Brillioun zone. The corrugated $Co\{11\bar{2}0\}$, and stepped $Co\{10\bar{1}2\}$ and $\{11\bar{2}4\}$ surfaces were used to model the effects of defect sites on different elementary steps. These surfaces were modeled using nine layers with the bottom three layers fixed at bulk positions. A 1x5x4 Monkhorst Pack[31] mesh is used to sample the surface leading to a k-point density grid of 0.05 $Å^{-1}$. The gas phase hydrocarbon intermediates (CH, CH_2, C_2H_3, C_2H) were optimized using spin polarized calculations in cubic supercells. The adsorbates are attached on one side of the slab and a vacuum layer of up to 10 Å is included within the supercell to avoid interactions between the neighboring cells.

The transition states for all of the reported reactions were located by using climbing nudged elastic band (NEB) method[31]. The normal mode vibrational frequencies are obtained for all the transition states a[32, 33] and the presence of a single imaginary frequency along the reaction coordinate confirms the transition state.

Kinetic Monte Carlo Simulations

The kinetic Monte Carlo simulations were carried out using a algorithms developed explicitly for this work as well as previous models and subroutines developed earlier[34-40]. The current algorithm uses a variable-time approach that simulates the temporal changes of the adsorbate layer, using a surface with periodic boundary conditions. A fairly comprehensive database was constructed from DFT-calculated binding energies for H, O, C, CH, CH_2, CH_3, CH_4 and C_2H_x intermediates, and overall reaction and activation energies for CO and H_2 activation, CH_x hydrogenation, and CH_x coupling reactions. This resulting database is considered the zero-coverage limit for the reactions considered. Lateral interactions are modeled by using more coarse-grained models to describe the interactions between different adsorbates. Lateral interactions are defined as either through-surface or through-space. Through-surface interactions are described as changes in the adsorption energies and reaction energies that arise from electronic interactions that

take place through the metal surface as the result of coadsorption. We have shown previously that these interactions and their influence on adsorption, reaction and activation energies can be modeled by using Bond Order Conservation (BOC) methods. [41-45] Through-space interactions are those that occur through space. These are typically steric type interactions that can be modeled by the inclusion of the electrostatic and van der Waals interactions from the Merck Molecular Force Field (MMFF94). [46, 47] Both the BOC algorithm as well as the MMFF algorithm can be called upon internal within the simulation to explicitly account for the effects of the local surface coverage.

For each time step, the barriers for all possible adsorption, desorption and surface reactions are computed. Using an Arrhenius relationship, the rate for each possible reaction is computed. One reaction is then chosen at random, with the probability of each reaction being proportional to the rate or each reaction. The time is advanced by choosing a second random number, and is inversely proportional to the total rate calculated, so that surfaces with larger total rates of reactions will be incremented by smaller time steps than surfaces with smaller total rates of reactions. Between steps, diffusion of all surface species is allowed to occur. This is assumed to be nearly instantaneous.

VI. RESULTS AND DISCUSSION

A. AB INITIO KINETIC DERIVED MECHANISTIC DATA

Herein we describe the ab initio results found for the elementary CO activation, CH_x hydrogenation, CH_x coupling reactions over ideal and stepped surfaces of Co and compare the results as well with those calculated over other metals.

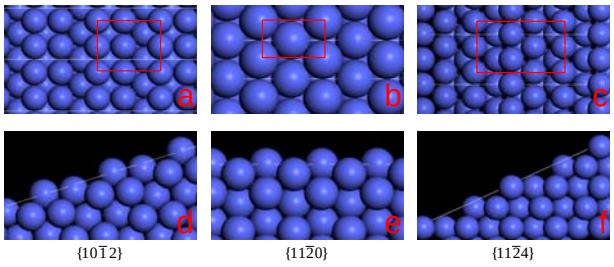

Figure 1. Top and side views of {10$\bar{1}$2}, {11$\bar{2}$0} and {11$\bar{2}$4} surfaces.

A.1. CO Activation

We have calculated in detail the adsorption and activation of CO using periodic plane wave DFT calculations within the generalized gradient approximation over the closed packed {0001}, corrugated {11$\bar{2}$0}, and stepped {10$\bar{1}$2} and {11$\bar{2}$4} surfaces of Co. [3] These optimized DFT structures for these surfaces are shown in Fig. 1. The calculated structure and energies for CO adsorption on these surfaces were found to be in very good agreement with experimental surface science results reported in the literature. The results are summarized below in Table 1. While the desorption of CO was calculated to be exothermic over all of the surfaces examined, its binding was found to be indifferent to the particular adsorption site as the energies changed by just a few kJ/mol regardless of the surface studied ranging from -160.4 to -164.6 kJ/mol.

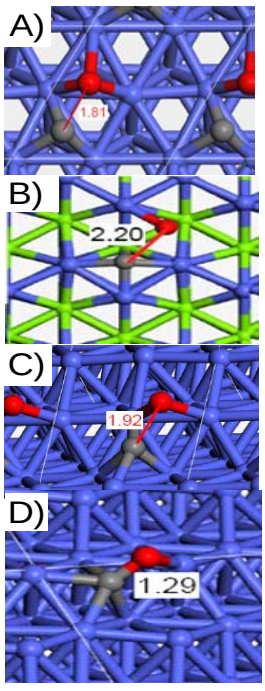

Fig. 2 DFT-calculated transition states for the activation of CO over closed packed {0001}, corrugated {11$\bar{2}$0}, and stepped {10$\bar{1}$2} and {11$\bar{2}$4} surfaces. [3]

The dissociation of CO on all these surfaces proceeds through a late transition state which has a pronounced C-O stretch with C-O distances that are between 1.8 and 2.2 Å. There is a strong interaction between the carbon and oxygen atoms with the metal surface. The activation barriers for CO were found to scale with the energy of the product state.

A. 2 Influence of Surface Structure on CO Activation

We examined the effect of surface structure on the adsorption and activation of CO over the {10$\bar{1}$2}, {11$\bar{2}$0} and {11$\bar{2}$4} surfaces of Co, all of which are known in the literature to be stable. [3]Each of which has a different degree of openness and coordinative unsaturation. Interestingly, we found that the surface structure did not appreciably affect the CO adsorption energy. Stepped surfaces, however, do provide more types of sites for CO adsorption, and in addition lead to more meta-stable adsorption configurations. High-coordination adsorption sites resulted in longer C-O bond in chemisorbed CO but the Co-CO chemisorption bond remained nearly the same.

If chemisorbed CO is used as reference state, the reactions over the

Co{0001} and Co{11$\bar{2}$0} become endothermic while those on Co{10$\bar{1}$2} and {11$\bar{2}$4} remain exothermic. The activation barrier for CO dissociation is thus sensitive to the actual surface structure. More open and stepped surfaces which provide stronger binding sites for the C and O adatoms favor CO dissociation. On Co{10$\bar{1}$2} and {11$\bar{2}$4}, pathways which have activation energies that lie below the gas phase CO at low coverages were identified. The existence of these low energy paths on the stepped surfaces allows a CO molecule from gas phase to dissociate spontaneously upon adsorption. This is consistent with the observed high reactivity of the stepped surface towards CO dissociation. The results here suggest that CO activation does not occur on the ideal {0001} terraces of Co but instead requires the presence of defect sites. This is consistent with recent experimental results from Shell for the hydrogenation of CO over Co(0001) [1] wherein they demonstrate that the activation of CO occurs at step edge defect sites.

Table 1. DFT calculated adsorption energies, reaction energies and activation barriers for CO over Co{0001}, Co{11$\bar{2}$0}, Co{10$\bar{1}$2}, and Co{11$\bar{2}$4} surfaces. [3]

	{0001}	{11$\bar{2}$0}	{10$\bar{1}$2}	{11$\bar{2}$4}
$\Delta E_{ads,CO}$	-160.4	-159.6	-164.6	-164.4
$\Delta E_{ads,C}$	-660.8	-684.4	-753.8	-716.6
$\Delta E_{ads,O}$	-544.0	-524.5	-576.9	-558.9
$\Delta E_{rxn,CO}$	**-100.3**	**-104.4**	**-226.2**	**-171.0**
$\Delta E_{act,CO}$	**72.5**	**40.0**	**-28.7**	**-48.5**

The more open and stepped surfaces provide strong binding sites for the C and O adatoms and are thus much more favorable for CO dissociation. The existence of low energy pathways on the stepped surfaces allows a CO molecule from gas phase to dissociate spontaneously upon adsorption. This is entirely consistent with the observed high reactivity of the stepped surface towards CO dissociation. [48-55]

A. 3. Coverage Effects

It is likely that the operating catalytic surface is covered with some form of hydrocarbon intermediate. What is on the surface under different reaction conditions, however, is still unknown and debated. The likely surface intermediates are CH_x fragments or adsorbed CO. The surface coverage was thought to have a very strong effect on the activation barriers for CO dissociation. We therefore examined the influence of coverage on the adsorption and activation of CO. As a first approach we simply explored the activation of CO at different initial CO coverages. More specifically we examined ($\sqrt{3}\times\sqrt{3}$)R30°, 2x2 and 3x3 unit cells in order to model the coverages of 1/3, 1/4 and 1/9 of a monolayer. The product states that form show a very strong coverage effect at the intermediate and higher coverages. For example, the repulsive interaction between C and O coadsorbed in a (2×2) surface unit cell is over 65 kJ/mol higher in energy than that of the C and O adatoms calculated separately in a (2×2) unit cell. Consequently, the overall reaction energy becomes less endothermic and the barrier decreases as we decrease the surface coverage. The overall reaction energy on the 2x2 surface was found to be endothermic by 130 kJ/mol with a barrier of ~230 kJ/mol. On the 3x3 surfaces, however, the overall energy becomes much less endothermic at 76 kJ/mol and the barrier decreases to 140 kJ/mol.

In general we found that the higher CO coverages inhibited CO activation as the result of lateral interactions. On all of the surfaces considered herein, the dissociation of CO is exothermic with respect to gas phase CO.

Table 2. DFT-calculated periodic trends in the reaction energy for CO activation and the carbon binding energy.

Metal	ΔE_{rxn} (kJ/mol)	E_B C (kJ/mol)
Co	-0.194	-6.305
Ni	-0.016	-6.428
Cu	2.792	-4.571
Ru	-0.533	-6.814
Rh	-0.128	-6.871
Pd	0.736	-6.645
Ag	5.461	-3.046
Os	-0.170	-6.661
Ir	0.355	-6.671
Pt	1.207	-6.567
Au	5.221	-3.925

A. 4 CO Activation – Periodic Trends

We can begin to extend the results on Co to other metals by systematically examining the effects that different metals have on carrying out specific elementary steps. The overall reaction energies on closed packed 3d, 4d, and 5d transition metal surfaces for CO activation with respect to the gas phase CO are reported in Table 2. The results are consistent with the well established trends cited earlier in that metals to the left in the period table can readily activate CO but tend to form carbides. For comparison, we have also listed the carbon binding energies which are stronger for metals on the left of the periodic table. The best metals from this table for activating CO are Co, Ru, Rh, Os and Ni which is consistent with the literature for FT synthesis.

More specifically we have examined and compared the barriers for the activation of CO over the ideal Co(0001) and Ru(0001) surfaces. The barrier to activate CO over Ru is 140 kJ/mol which is 40 kJ/mol lower than that found over Co which was 230 kJ/mol. This is consistent with the stronger binding energies reported above in Table 2.

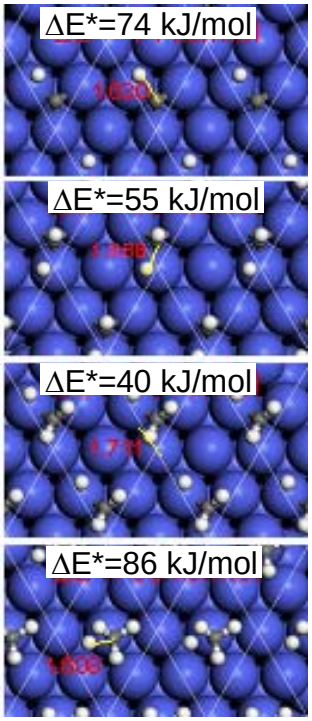

Fig. 3. DFT-calculated transition states and activation barriers for the hydrogen addition to C*, CH*, CH_2*, CH_3*.

A. 5. Hydrogenation of CH_X Fragments

The carbon atoms that form as the result of CO activation are sequentially hydrogenated to form CH^* CH_2^*, CH_3^* intermediates. We have systematically examined each of these reactions over Co{0001} as well as other closed packed metal surfaces. The adsorbed CH^* was found to be the most stable surface intermediate over Co. The transition states for C^*+H^*, CH^*+H^*, $CH_2^*+H^*$, $CH_3^*+H^*$ are shown in Fig. 3. The addition of the first hydrogen to the adsorbed C* to form CH^* and the last hydrogen to CH_3^* to form methane were found to be the most difficult steps in the process. The addition of hydrogen to the adsorbed CH_x intermediate involves the insertion of hydrogen into the metal carbon bond. The transition state which is shown in more closeup detail in Fig. 4 reveals the characteristic early transition state for most hydrogen additions. There is a long carbon-hydrogen bond and a relatively short metal-hydrogen and metal-carbon bonds. As

discussed above, the first step in hydrogenating C to methane as well as the last are the most difficult. The results suggest that the addition of the first hydrogen to form CH* and the last hydrogen to CH_3* to form methane have barriers of 74 and 86 kJ/mol respectively which are the limiting for the hydrogenation sequence of steps. They are, however, significantly lower than the barrier for CO activation over Co(0001).

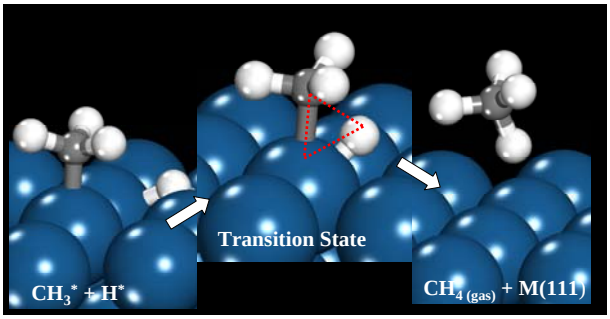

Fig. 4 The reaction path for the hydrogenation of CH_3* to methane.

These results were subsequently extended to other metal surfaces in order to examine the influence of the metal on the energetics. The overall reaction energies along with the corresponding activation barriers for the hydrogenation of CO to methane over a range of different metals were calculated for comparison purposes. The addition of hydrogen to an adsorbed CH_x^* intermediate is simply the microscopic-reverse of the activation of the C-H bond within the CH_{x+1}species. The resulting potential energy diagram for the activation of methane to adsorbed C (i.e. the reverse of the addition of hydrogen to C to form methane) diagram is shown in detail in Fig. 5. The results suggest that the barrier to activate the C-H bond in methane to CH_3 may be related to the heat of reaction through an Evans-Polanyi relationship. A closer analysis reveals that indeed the barriers scale linearly with the elementary energies of reaction. An Evans-Polanyi relationship, therefore, nicely captures the kinetics for C-H bond activation over a range of different metals as is seen in Fig. 6. We have taken this correlation one step further in that depending upon the adsorption strength of the reactants and the products one of them will tend to dominate. Therefore the activation barriers can be correlated with the heats of adsorption of the reactant or product states. We can use this idea to more rapidly establish the activation barriers over different alloy substrates by simply calculating the CH_x*

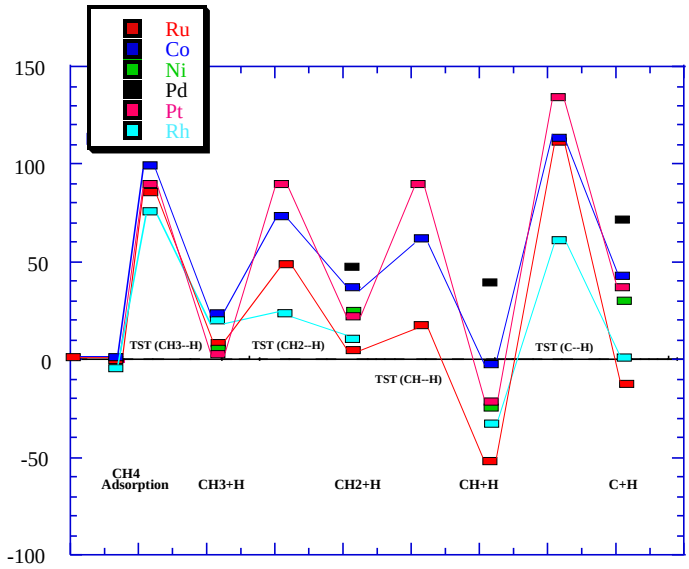

Fig. 5. DFT Calculated potential energy path for CH_4 activation to CH_3, CH_2, CH and C over different metals.

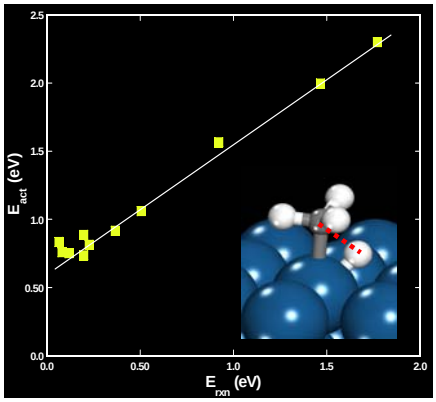

Fig. 6. DFT calculated Evans-Polanyi relationship for the activation barrier for methane activation over different transition metals.

and potentially the H* binding energies on them.

The results here provide a fairly comprehensive data base for the hydrogenation of CH_x* intermediates. The results also provide an important database of kinetics for methane activation over different metal substrates. The results can therefore also be used to understand the activation of natural gas.

A. 6. Carbon-Carbon Coupling

The selectivity to higher hydrocarbon products ultimately resides on the balance between CH_x* hydrogenation and hydrocarbon coupling. Faster rates of CH_x coupling ultimately result in the production of higher MW hydrocarbons. In order to fully understand selectivity it is important to first elucidate the intrinsic kinetics over idealized substrates. Our calculated results over the ideal Co{0001} surface indicate that the barriers for hydrocarbon coupling show the following trends: CH*+CH* > CH*+CH_2* > CH_2*+CH_2* > CH_2*-CH_3*. Our results suggest from CH_x* hydrogenation suggest that the CH* intermediate is the most stable species and is likely the most predominant species on the surface. Therefore one of the more likely reaction paths would involve the coupling of CH* and CH_2* which is shown in Fig. 7.

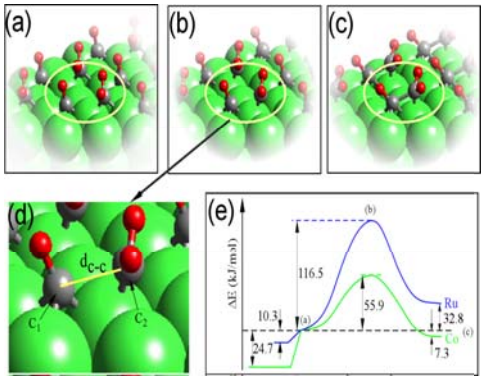

Fig. 7 Comparison of DFT calculated coupling of CH* and CH_2* over Co and Ru. [2]

The carbon-carbon coupling reaction has long been debated in the literature. Detailed kinetic isotope experiments performed by had resolved the issue that CO is activated to C* and O*[15-17, 56, 57] on the surface that is thought to initiate chain growth. Based on these studies it was believed that monomer involved in chain growth was the carbon atoms or CHx species that are formed on the surface. There is growing speculation that CO is the actual monomer and the carbon is necessary perhaps to just initiate the chain. This has re-opened the debate as to the active carbon intermediate. We return to this point later in the discussion.

A.7. Carbon-Carbon Coupling Along Step Edges

We have shown above that the CO bond readily activates at the step sites. It has been speculated that these are also the sites which favor the carbon-carbon coupling reactions. We have therefore examined in detail the adsorption of the different CH_x intermediates on the Co{10$\bar{1}$2} surface along with the overall reaction energies and the activation barriers. The detailed breakdown of the most favorable adsorption sites for each of these intermediates is given in the Appendix.

A.7.1. Methylidyne (CH) Adsorption on Co{10$\bar{1}$2}

Methylidyne (CH) is bound via carbon to the various adsorption sites considered in Fig. 8. The adsorption energies at each of these sites are summarized in Table A1 in the appendix. The four-fold hollow sites (J and K) were found to be the most stable. They were closely followed by the four-fold bridging and three-fold hollow adsorption sites. The atop and bridging CH was bound much more weakly to the atop and bridging adsorption sites. The adsorption of CH on the 4-fold site J and the bridge site D is shown in Fig. 9

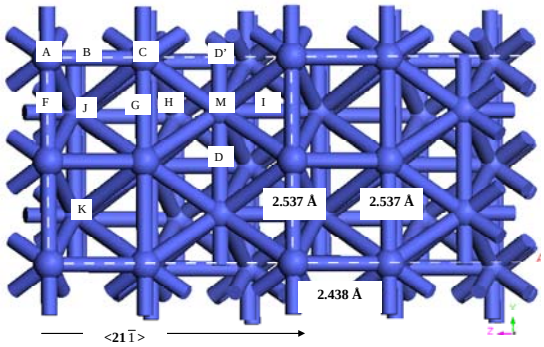

Figure 8. Top view of the Co{10$\bar{1}$2} surface with the adsorption sites considered

A.7.2 Methylene (CH_2) on Co{10$\bar{1}$2}

The adsorption energies and bond distances for the stable adsorption geometries of CH_2 bonded to the step edged Co{10$\bar{1}$2} surface are summarized in Table A2 in the appendix. As might be expected the adsorption energies for methylene are significantly lower than those for methylidyne. Similar to methylidyne, methylene was also found to adsorb much more strongly to the four-fold hollow sites with adsorption energy of -4.1 eV. This was followed by bridging sites and three-fold hollow sites.

The adsorption geometries considered include structures with the C-H bonds of the adsorbed CH_2 lying in (010) plane, twisted normally with respect to the adsorbed CH_2 with C-H bonds lying in (21$\bar{1}$) plane. Both these orientations results in comparable adsorption energies of -2.86 eV for adsorption of CH_2 on atop site C. The twisted orientation of CH_2 with C-H bonds in (010) plane adsorbs on atop site A with a stronger bond with the surface cobalt atom and binding energy of -3.16 eV. The CH_2 adsorbate is in a stable tetrahedral orientation when adsorbing on bridge sites on Co{10$\bar{1}$2} surface and hence, no twisted configurations are considered for CH_2 adsorbed on bridge sites.

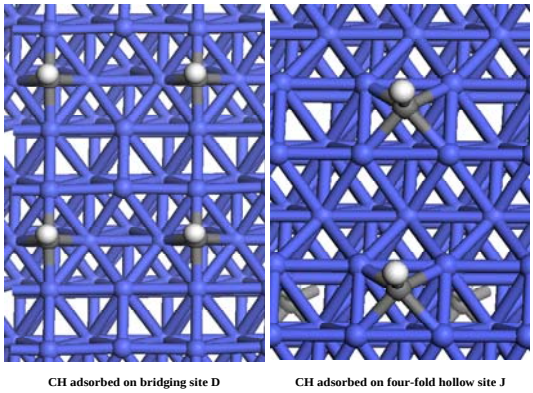

Figure 9. Top view of the Co{10$\bar{1}$2} surface with CH adsorbed at bridging site D and four-fold site J.

A.7.3. CH and CH_2 coupling reaction pathways

The CH-CH_2 coupling reaction involves a trade off between maximizing the adsorption energies and minimizing the activation barriers. The CH intermediate binds nearly 2.5 eV more strongly to the Co{10$\bar{1}$2} surface as compared to the CH_2 intermediate and is therefore, much less mobile. Four-fold hollow sites are found to be most favorable sites with adsorption energies of -6.7 and -4.1 eV for CH and CH_2 respectively. These two intermediates are co-adsorbed in different sites and the stable configurations are reported in Table A3 in the appendix. The vinyl product (C_2H_3) that forms also adsorbs quite favorably in various configurations on Co{10$\bar{1}$2} surface. The results are detailed in Table A4 of the appendix. The most stable adsorption geometry for the C_2H_3 intermediate is one where the carbon termini of CH and CH_2 adsorb on the bridge sites F and G on Co{10$\bar{1}$2} surface.

Route	Co-adsorbed Reactants		Product C_2H_3	E_{rxn} (eV)	Ea (eV)
	CH	CH_2			
1	J	I	G-F	-0.02765	1.123617
2	J	M	F-G	-0.05168	0.943273
3	D	J	G-F	-0.05329	1.214181

Table 3. DFT calculated reaction energies and activation barriers for CH + CH2 coupling over Co{10$\bar{1}$2}.

The most stable adsorption sites were found to lead to fairly high overall reaction energies and activation barriers. In addition to these high energy paths we explored the more favorable routes tabulated in Table 3 above. These routes included co-adsorbed CH and CH_2 on hollow and bridging sites and C_2H_3 on the most stable adsorption sites.

The coupling of CH and CH_2 on the Co{10$\bar{1}$2} surface ws found to be slightly exothermic for all the routes considered. In addition, the lowest energy activation barriers were all found to be approximately 1 eV over the Co{10$\bar{1}$2} surface. These activation barriers are nearly two times higher than that for the CH* and CH_2* coupling over the Co(0001) flat surface (0.55 eV) (the transition state was shown back in Fig. 7). The activation barrier for route 1 over the Co{10$\bar{1}$2} where CH resides on the four-fold hollow site J while CH_2 climbs up to the terrace from the three-fold hollow site I to form C_2H_3 was calculated to be 1.12 eV. The co-adsorbed CH and CH_2 share two cobalt atoms in the surface which ultimately leads to a high barrier as the result of the repulsive interactions that occur for metal-atom sharing. The barrier reduces slightly to a value of 0.94 eV for route 2 where CH_2 goes up a lower slope terrace to add to CH on the four-fold

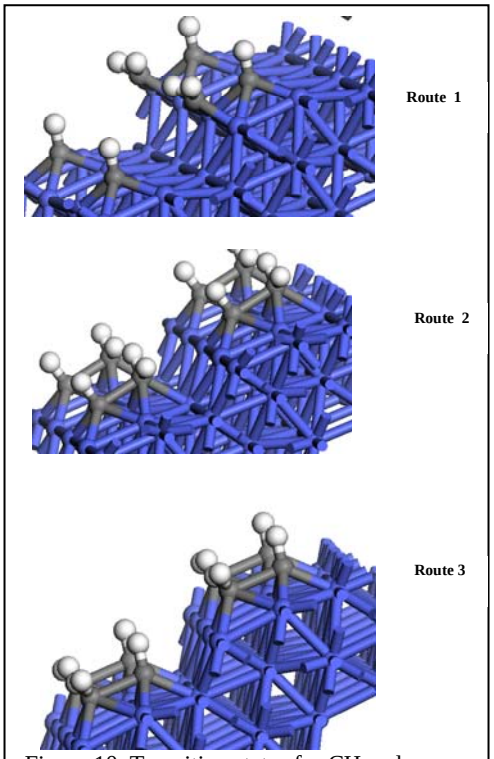

Figure 10. Transition states for CH and CH_2 coupling reaction on the steps of Co{10$\bar{1}$2

site in order to react and form vinyl in the configuration of F-G. The barrier for the coupling reaction was calculated to be 1.21 eV for the case where CH transitions from a bridging site up a lower slope terrace to form vinyl product.

The CH and CH_2 coupling reaction is also reported to have a higher energy barrier for Ru stepped surface as compared to the flat Ru(0001) surface [58]. It was concluded that $C+CH_x$ reactions are the favorable pathways for chain propagation. Hence, we consider CH and C coupling reaction on Co{$10\bar{1}2$} surface in the next section with CH intermediate being more mobile than C adatom.

A.7.4. CH and C reaction pathways

The binding of the carbon adatom on Co{$10\bar{1}2$} surface has been reported to be stable for four-fold hollow sites and bridging site [3]. The DFT based adsorption energy for carbon bonded to the four-fold hollow site J is -7.5 eV. There is significant reconstruction for the adsorption of carbon at these sites on the stepped cobalt surface. The adsorption of carbon on the bridging site D is reported to be stable with adsorption energy of -6.9 eV. The most stable adsorption energy for the C_2H product was found to be -5.8 eV with the C terminus of the CH subset binding to the bridge site F and the other C terminus binding to four-fold site J.

Route	Co-adsorbed Reactants		Product C_2H	E_{rxn} (eV)	Ea (eV)
	CH	C			
1	J	M	F-J	-0.54933	2.19
2	M	J	F-J	-0.26588	1.35
3	J	M	G-M	0.08129	1.51

Table 4. Reaction energies and activation barriers for CH and C coupling on Co{$10\bar{1}2$} surface.

The pathways considered for the coupling of CH and C are tabulated here in Table 4 and the transition states are shown in Fig. 11. The activation energy barriers for all the routes considered were found to be 1.5 eV or higher. Route 1 involves the tranistion of CH from four-fold hollow site J to the bridge site F while forming a C-C bond with C adatom moving from the stable bridging site over the low slope terrace to the stable four-fold site. This path, however, had the highest barrier of the three paths studied at 2.19 eV. In the second path examined, the CH intermediate was bound to bridging site in the initial configuration while the C atom was initial bound to the stable four-fold site J. The final C_2H product is formed when CH moves over the step to the bridge site F. The calculated barrier for this path was 1.35 eV. Both routes 1 and 2 were calculated to be exothermic with stable C_2H product structures. The third

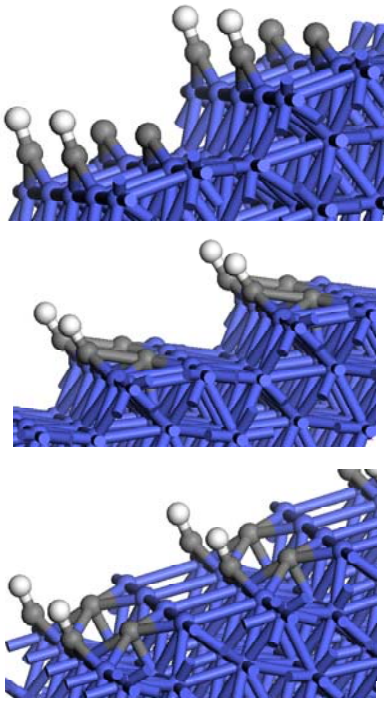

Figure 11. Transition states for CH and C coupling reaction on the steps of Co{$10\bar{1}2$}

reaction path examined was found to be nearly thermoneutral a reaction energy of 0.08 eV. This pathway has a reaction barrier of 1.51 eV and includes transition of CH down the slope from four-fold site J to the bridge site G in order to form C_2H. The high activation barriers calculated here for the C* and CH* coupling can be partly attributed to the sharing of metal atoms on the surface between the co-adsorbed intermediates.

A.8. Water Formation/Dissociation

The water that is formed during the conversion of H_2/CO to hydrocarbons can increase the reaction rates, as well as the molecular weight and olefin content in the products [7, 59]. Higher water concentrations, however, can also lead to the irreversible oxidation of smaller Co crystallites and a significant loss in their catalytic activity. The influence of water depends on the sites where it forms. The more coordinatively-unsaturated sites will activate water with a much lower barrier. The presence of oxygen at these sites may ultimately form a surface oxide since the binding energy of oxygen at the edge and corner sites is significantly higher than on the terrace sites. Smaller particles, which have higher concentrations of coordinatively-unsaturated sites, will have a greater tendency to form oxides. As a very first step towards understanding the effects of water, we studied the adsorption and stability of water on Co{0001}. Water was found to adsorb with an energy of 36.3 kJ/mol. The calculations also indicate that water dissociates over Co{0001} with an overall energy of -49.2 kJ/mol, and with a barrier less than 10 kJ/mol. The activation barrier for the formation of water over on the Co{0001) surface is the microscopic reverse resulting in a barrier of 59.2 kJ/mol. Consequently, water formed during syngas reactions will most likely exist as coadsorbed hydroxyl groups and hydrogen adatoms, depending on the partial pressure of water and hydrogen.

A.9. The Influence of Alloying Co with Ru: CO Adsorption and Dissociation

Ruthenium is often used as a promoter in Co-based catalysts and has been proven to effectively improve the activity of the catalysts [7, 8, 21]. However, Ru is a rare element and only mined with other precious metals in small quantities. Therefore, understanding the mechanism with which Ru promotes a Co-based catalyst is both economically and scientifically important. In the this work, we studied CO adsorption on uniform Ru-Co surface alloys supported on both Co and Ru substrates to examine the effect of the presence of a second metal, in particular when they form a surface alloy, on the strength of the CO-surface bond and on the reaction pathways. The adsorption calculation has been performed with a $(\sqrt{3}\times\sqrt{3})R30°$ unit cell. The calculated CO adsorption energies on various sites at different surface compositions are listed in Table 5. We note that the binding energy of CO on Co sites over the surface alloy formed on Ru substrate is greatly increased with respect to that on the pure Co surface. On the other hand, the CO chemisorption bond is slightly weakened on the Co site over the surface alloys supported on a Co substrate. This can be explained as Co has a smaller lattice spacing than Ru and supporting a surface alloy of Co-Ru induces strain within the layer of the surface alloy. The small distance between Co and Ru may cause a charge redistribution between Co and Ru. The charge transfer from Ru to Co will impede the ability of Co to accept charge

Table 5. CO adsorption energies on Co-Ru surface alloys, in kJ/mol

Composition		0.33	0.66	1.00
Co on Ru	Co site	182	186	181 (top)
	Ru site	198	205	179 (hcp)
Ru on Co	Co site	153	143	145 (hcp)
	Ru site	190	173	205 (top)

from a CO molecule, and consequently weakens the chemisorption bond of CO formed on the Co site.[60] We also started to examine CO dissociation over the surface alloys. Our results showed that CO dissociation can be exothermic over the surface alloys. For example, CO dissociation over the Co site on Co-Ru surface alloy supported on Ru substrate at a Co composition of 0.33 is exothermic with heats of reaction of -10.8 kJ/mol.

The strong C and O bond to Ru ultimately enhance its ability to activate CO. The strong Ru-C and Ru-O bonds however allow Ru to bind the C and O surface intermediates too strong and thus make Ru less active for hydrogenation and hydrocarbon coupling. The hydrogenation paths shown earlier in Fig. 5 and summarized here in Table 6 indicate that the barriers for the hydrogenation of C all the way to methane are systematically higher over Co than over Ru.

Table 6. Dissociation energies of methane to different products over Co{0001} and Ru{0001} in kJ/mol.

Reaction	Co	Ru*
$C_a + H_a \rightarrow CH_a$	74	105
$CH_a + H_a \rightarrow CH_{2,a}$	55	70
$CH_{2,a} + H_a \rightarrow CH_{3,a}$	40	45
$C_{3,a} + H_a \rightarrow CH_4$	86	90

Similarly, the barriers for carbon-carbon coupling are also higher over Ru than over Co. This is shown above in Fig. 7 for the reaction of CH* + CH_2*. The barrier over Ru is over 60 kJ/mol higher. Ru therefore likely aids in CO activation but the hydrogenation preferentially appears to occur over Co.

A.10. Summary of Ab Initio Work

We have established a fairly comprehensive database on the heats of adsorption, the activation barriers and the overall reaction energies for the dominant elementary steps which control the initial pathways in the synthesis of longer hydrocarbons. It is clear from the results that there are many different surface structures and compositions that can form thus challenging the use of ab inito theory to calculate all of the conceivable reaction pathways, the surface coverages and site dependences. We can, however, build structure-property relationships that begin to capture the most essential features. From the results, it is also quite clear that many of these processes display similar activation barriers. The prediction of the impact on catalytic performance is impossible without the aid of a kinetic model to establish the appropriate surface coverages that result at actual reaction conditions. To this end we have focused our effort on the development of a stochastic kinetic approach which allows us to keep the surface structure explicit and utilize the wealth of information derived from the ab initio results.

B. KINETIC MONTE CARLO SIMULATION

B.1. KMC Approach

The ab initio results described above can be used in order to begin to simulate kinetics. Deterministic microkinetic models can be used to simulate the kinetics but they rely on averaging over the surface coverage in order to provide surface concentrations. Our goal in

this work was to try to maintain the atomic surface structure which could ultimately aid in catalyst design efforts. As such we instead used stochastic kinetics in order to simulate the kinetics of FT synthesis. As such we developed a Dynamic Monte Carlo Simulation algorithm which can simulate the initial kinetics for FT.

The simulation was described in detail in previous report. Herein, I describe only some of the salient features. The basic input to the simulation can be divided into three main areas: 1) the lattice (size and structure), 2) molecular data on the all of the reactants, intermediates and products (geometric structure, atomization energies, etc.), and 3) intrinsic kinetic data (activation barriers, pre-exponential constants, adsorption energies, overall reaction energies). This structure of the code is taken from previous KMC codes that we have written and is [34-40] shown schematically in Fig. 12.

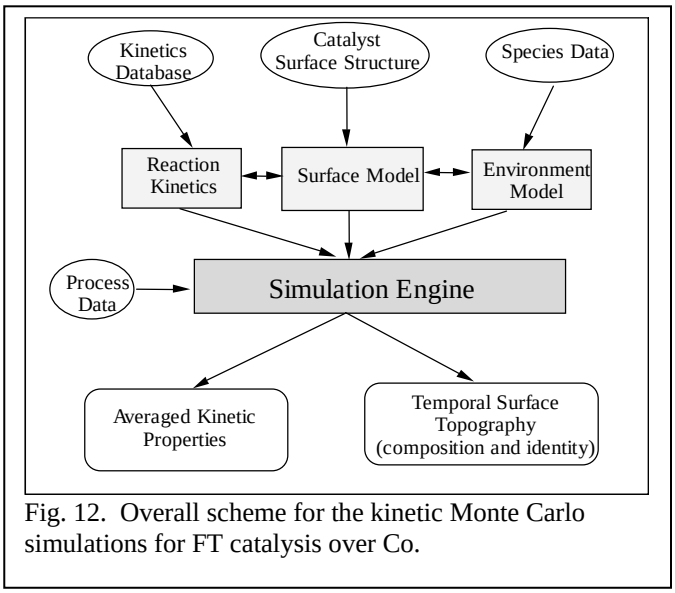

Fig. 12. Overall scheme for the kinetic Monte Carlo simulations for FT catalysis over Co.

The current code was developed to simulate the initial steps for Fischer Tropsch synthesis over close-packed, (0001) or (111) surfaces as well as more open (100) surfaces. The catalytic surface is described in the simulation by a periodic MxM lattice where M defines the number of atoms along each edge of the repeating cell. The simulations can explicitly track atop, bridge, and higher-fold coordination sites and the fate of the adsorbates bound to these sites. The lattice is atomically explicit to enable us to fully capture the influence of the local reaction environment on the kinetics. The user can specify the size of the grid. Computational constraints typically limit grid sizes to 100x100 or 200x2000. We usually run a grid of at least 24x24 and average over several replicates. The results on these smaller grids tend to match up reasonably well with larger grid sizes.

The molecular or species input data refers to a set of general molecular properties for all of the possible reactants, intermediates and products within the simulation. This includes the adsorbate's binding energy at specific sites on the surface, van der Waals radius (physical size), gas phase dissociation energies and geometric structure.

The intrinsic kinetic database is compiled from the ab initio results that have been developed over the course of this effort on CO activation, CH_x hydrogenation and coupling reactions over the Co(0001) surface. The current reaction database is currently being extended to provide for a complete description of not just the Co(0001) surface but other surfaces and the influence of steps and defect sites.

The input data is subsequently used to construct a surface simulation model that incorporates the intrinsic reaction kinetics along with adsorbate-adsorbate interactions that occur on the surface via through-surface and through-space lateral interactions. This enables us to explicitly treat the effects of the reaction environment on the kinetics. These models of the surface, molecules and intermediates, and reaction kinetics and environment comprise the basic modules of the simulation.

B. 2. Simulation Results

The kinetic Monte Carlo simulations reveal rather interesting and informative results. The bare Co surface here was initially exposed to a gas phase which contains a constant partial pressure of CO and H_2 at a constant temperature. There is an initial transient whereby hydrogen readily dissociates over the bare metal surface to form atomically adsorbed hydrogen, H*. CO adsorbs initially but the rate is lower than that for H_2. CO, however is more favored and at some point begins to build up on the surface and ultimately begins to displace the atomic hydrogen. The surface at longer times is covered in CO reaching a surface coverages of about 0.5 ML. The dissociation of hydrogen becomes somewhat more inhibited. The hydrogen that forms readily reacts with the CH_x* intermediates. The steady state coverage of hydrogen then is fairly low at about .01 ML. CH* ultimately becomes the dominant species, thus reaching a total surface coverage of 0.1 ML by 10^{-7} seconds,

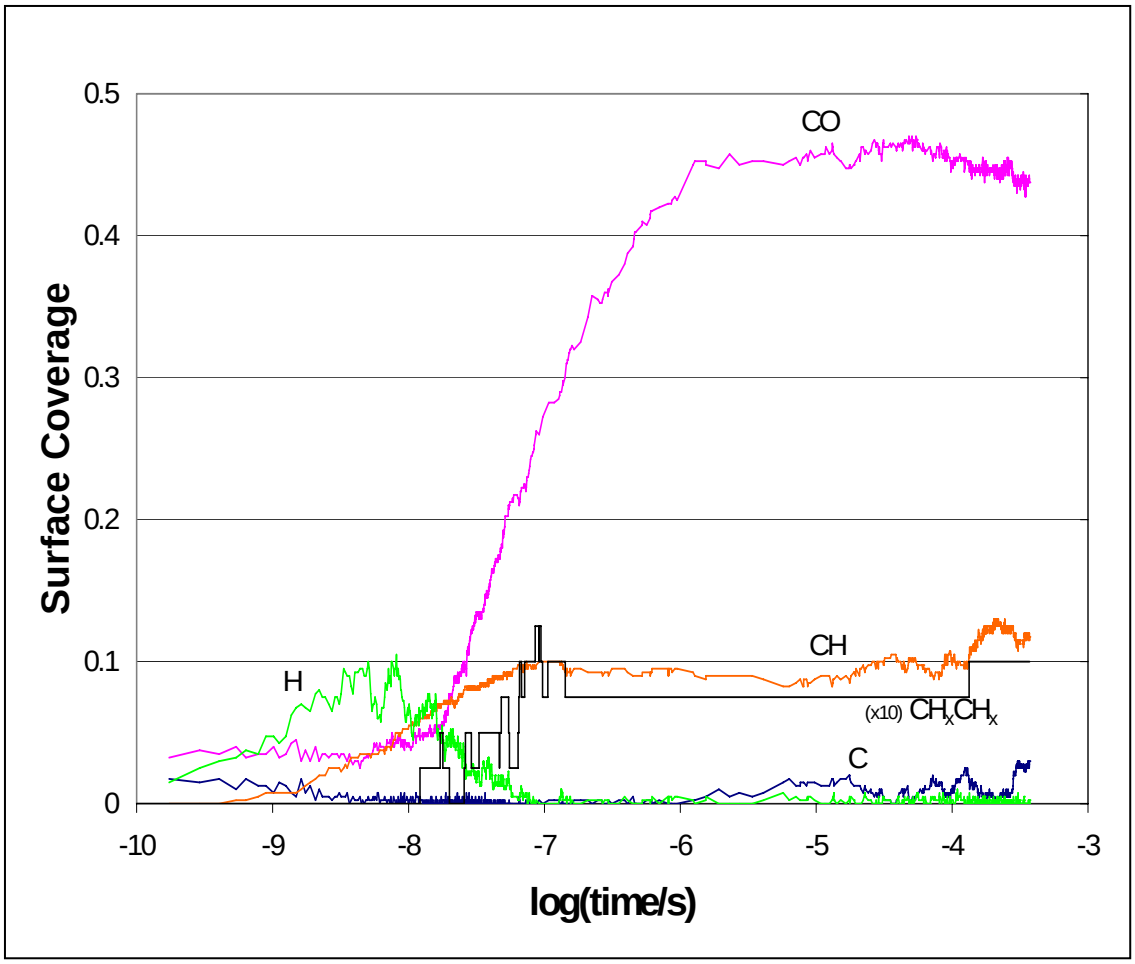

Fig. 13. Kinetic Monte Carlo simulations for the conversion of CO and H2. Simulated surface coverages.

While the overall thermodynamic reaction energies, would indicate that the CH_3* should be the most abundant CH_x* species that forms on the surface, the simulations show that CH* is the most abundant CH_x^* intermediate. The coverages of C* and CH_2* follow that of CH* but they are only 0.005 ML and 0.02 ML respectively. This can be understood from the kinetics for the hydrogenation reactions presented earlier in Fig. 3 and Fig. 5. There is only a small barrier to hydrogenate C* to form CH*. The barrier to hydrogenate CH* to form CH_2* is roughly the same as the barrier to dehydrogenate CH* to form C* and H*.

A snapshot of the surface coverges is shown in Fig. 13. It reveals that the surface is predominantly covered with CO. CO activation appears to be the rate determining step. CO, which is strongly bound to the surface acts to block sites and thus slows down the rate for all CH_x coupling and CO dissociation reactions. This implies that the CH_x^* + CO^* coupling reactions may also be important. This was also recently suggested by Shell as well.

The barrier to form CH_3* from CH_2* and H* is roughly similar to the barrier to form CH_2* from CH* and H*. However, because the surface coverage of CH_2* is significantly lower than the coverage of CH*, we find that the surface coverage of CH_3* is actually much lower. The rates of course are controlled not only by the barriers but also by the surface coverages.

Finally, the barrier for the hydrogenation of surface CH_3* intermediates with H* to form methane is significantly higher than the other hydrogenation barriers. The high barriers, combined with the lower surface coverage of CH_3* ultimately results in the negligible formation of CH_4 in the simulations.

The simulations result in the formation of C_2H_x* surface intermediates. The reactions of CH* + CH_2* and CH* + CH_3* were the only carbon-carbon coupling reactions seen within the simulation. The CH_2* coverage was low enough that CH_2* + CH_2* never occurred. Once the C_2H_x* species were formed, they typically underwent hydrogenation reaction and dehydrogenation reactions to lead to the formation of chain terminating products. Some underwent decoupling reactions to form CH_x* + CH_y* species, although this was much less common. Subsequent hydrocarbon coupling reactions were not included yet into the code as we wanted to isolate and understand the reactions which control C_2 formation.

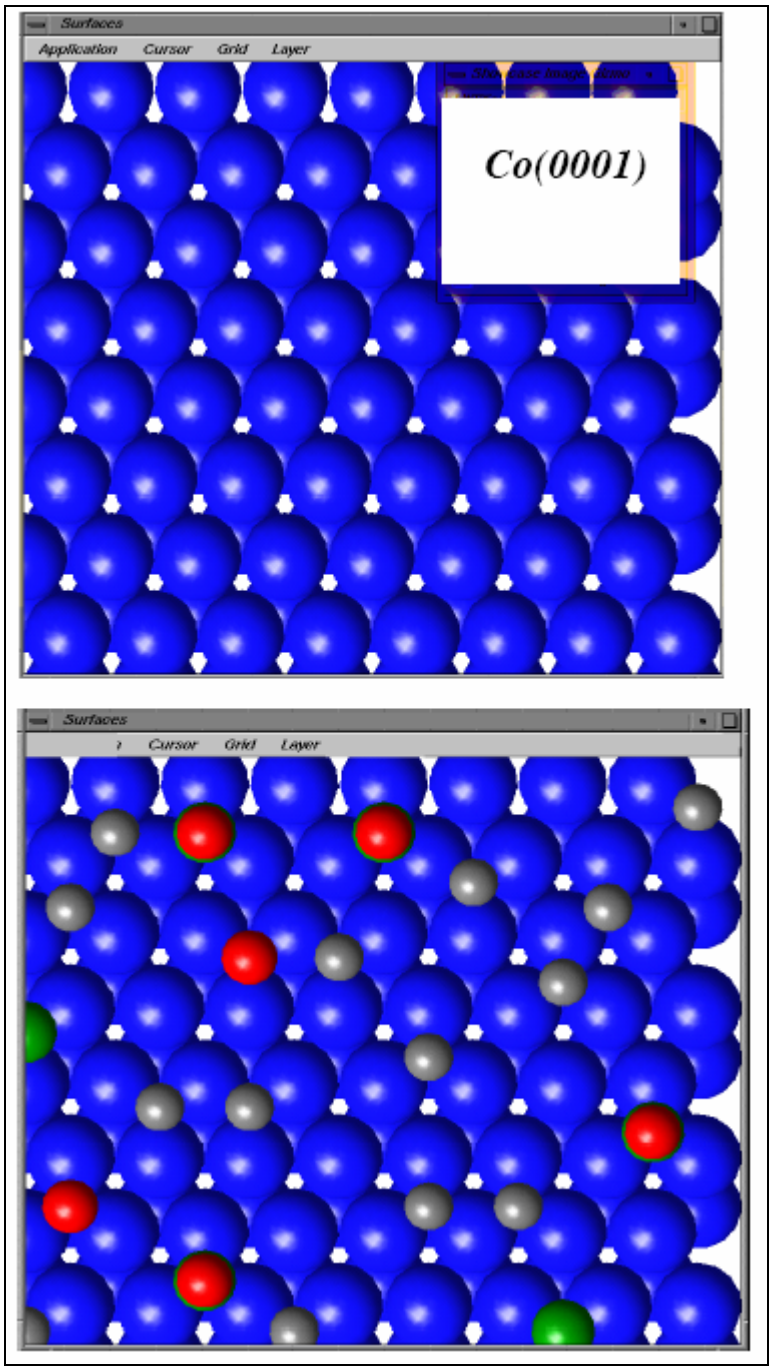

Fig. 14. Snapshot taken of: A) the initial Co(0001) surface, and B) the covered surface taken at a short time after the reaction began. (Red spheres are oxygen atoms, green spheres are carbon, and gray spheres are hydrogen atoms.

C. DISCUSSION

What is clear from the ab initio results as well as from the DFT results is that the reaction appears to be controlled by the barrier for CO activation as well as the availability of free sites on the surface. The intrinsic barrier to activate CO at higher surface coverages on the (0001) terraces is over +230 kJ/mol. While the barrier on the terrace is reduced to 70 kJ/mol, it requires coverages on the order of 1/9. The simulations show that while individual vacant sites open up within the adlayer, large vacant ensembles will only very seldomly form. The activation of CO at the step sites is much more favorable with barriers that are less than 40 kJ/mol. This would suggest that the step sites are the active sites for CO activation. This result is nicely supported by the in-situ STM data reported by Shell [1]that is presented in Fig. 15. The data show that the active sites are those that occur along the step edge.

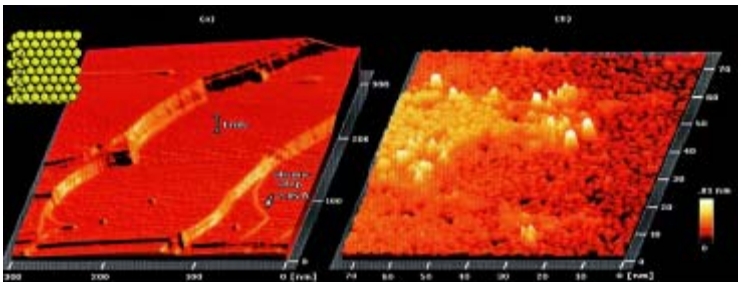

Fig. 15. STM snapshots of a) the clean Co(0001) surface with a single step edge defect. B) the resultant surface after 1 hour exposed to syngas From [1] at 523 K.

The questions about "where does the carbon-carbon coupling proceed?" and "what are the active species that drive the reaction?" are still debated. Our results would suggest that CO is activated at the step or defect sites and subsequently hydrogenates at these sites or diffuses to the terraces where they can hydrogenate more rapidly. As such, the active CHx* intermediates must be able to diffuse away from the step edge where they are formed. We have not calculated these barriers yet. However, simple estimates from Bond Order Conservation would suggest that the barriers would not be as high as those for CO activation or CH_x coupling. The kMC simulations show that the CH_x species build up on both the step edges as well as on the 0001 terrace. Coupling appears to occur most favorably at the terrace sites. The barriers for all of the CH_x intermediates at the step and more corrugated surfaces were found to be over 30 kJ/mol higher than those on the terrace sites. This point is still, however, under debate. The work by Shell suggests that the coupling predominantly occurs at the step edge sites. They suggest, however, that the coupling that occurs is actual the insertion of CO into a CH_x that has initially formed via the activation of CO to surface carbon. We are currently examining the coupling of CO and different CH_x intermediates at both the step as well as the terrace sites. This information will provide a more detailed understanding the elementary steps that control FT synthesis.

Newer Avenues/Future Directions

Methanol and Ethanol Synthesis

Much of the work on FT synthesis has been targeted toward the development of middle distillate fuels, heating oils and other hydrocarbon products. There has been some studies however which have shown that over certain metals one can produce oxygenates [61-65]. As discussed earlier, metals to the right in the periodic table have difficulty dissociating the CO bond and as such are typically good materials for carrying out hydrogenation reactions

necessary for methanol production. Cu [58] and Pd [61] for example are typically well known for catalyzing the hydrogenation of CO to methanol.

There have also been a number of studies which indicate that Rh is active in the production of ethanol. This is of no surprise since cationic Rh complexes are used as the commercial catalyst for hydroformulation processes. We hope to extend our efforts here for FT to hydrocarbons to FT to oxygenates for future efforts. If one could control the selectivity of this process, it could offer significant benefits to the enzymatic routes to ethanol currently employed.

Table 7. DFT calculated overall reaction energies for the hydrogenation of CO to methanol.

$CO + 2H_2 \rightarrow CH_3OH$

Surface Alloys		*Pseudomorphic Overlayers*	
Ru-Pt(111)	-0.55	Pt/Ru(0001)	-0.86
Pt-Ru(0001)	-0.72	Pt/Pd(111)	-0.23
Cu-Ir(111)	-0.29	Pt/Au(111)	0.02
Ir-Cu(111)	-0.01	Cu/Zn(0001)	-1.30
Sn-Pt(111)	-1.15	Au/Cd(0001)	-1.70
Ni-Pt(111)	-0.50	Ir/Cu(111)	-0.15
Ag-Pt(111)	-0.43	Pt/Al(111)	-0.19
Pt-Au(111)	-0.66		
$Pt_{66}Ru_{33}$/Ru(0001)	-0.71		

As discussed in the introduction, the paths that control syngas chemistry depend strongly on the intrinsic kinetics of both bond-making (C-H, C-C and O-H) and bond-breaking (C-O, H-H) surface processes as well as the explicit surface coverages of the different intermediates present. We can ultimately use much of the data that we have generated the hydrogenation of CO as well as the other pathways for FT to examine the synthesis of methanol or ethanol. We have examined in detail various processes for the hydrogenation of CO to methanol. The best metals tend to be those which lie further to the left as they result in the weakest metal-carbon and metal-hydrogen bonds. Both Cu and Pd as discussed tend to quite effective and have been shown to work reasonably well experimentally. We subsequently extended these studies to range of surface alloys as well as pseudomorphic overlayers in order to find more active bimetallic systems. The overall reaction energies over some of these surfaces are given in Table 7. The Sn-Pt(111), Cu/Zn(001) and Au/Cd(0001) all appear to be highly exothermic. CuZnO is used commercially [58] to produce methanol via CO hydrogenation. The Sn-Pt(111) and the Au/Cd(0001) systems may be interesting systems to examine. Much more work will certainly need to be explored.

In addition to examining the paths to CO hydrogenation, we have also examined the C-H bond activation pathways for ethanol decomposition over both Pt(111) as well as Rh(111) surfaces. The overall potential energy profile for ethanol dehydrogenation to CO and hydrogen over Pt(111), which is simply the microscopic reverse of ethanol synthesis, has been calculated. The results suggest that it is significantly easier to break the C-H bond over the O-H bond of adsorbed ethanol. The activation of the secondary C-H bond is much more favorable than the primary C-H bond. The reaction then proceeds via the sequential activation of C-H bonds. The activation of the O-H, C-C, and C-O bonds are much less favorable than C-H bond activation. Breaking the C-C bonds of the more saturated CH_x groups is much less favorable than the activation of the C-C bond for the unsaturated carbon centers. The overall energies calculated for both C-H and C-C bond breaking appear to be much more favorable over Rh(111) than over Pt(111). The results for ethanol decomposition

over Pt(111) are shown in Fig. 16. We are currently completing the barriers for these paths as well as the C-O bond breaking paths over both the Pt(111) and Rh(111) surfaces. Subsequent studies will be completed over a range of different metals in order to establish periodic trends.

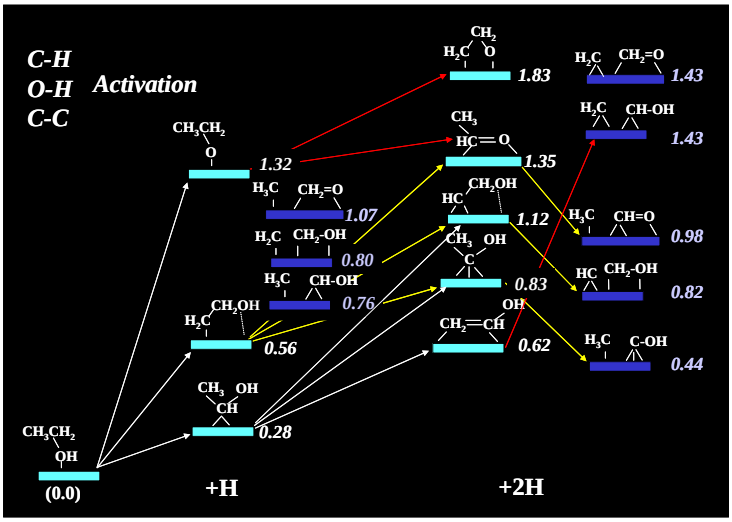

Fig. 16 DFT calculated reaction energies for the decomposition of ethanol to CO and hydrogen over Pt(111).

VII. CONCLUSIONS

The work completed in this DOE grant has resulted in a fairly comprehensive database for the elementary steps involved in Fischer-Tropsch synthesis over Co as well as CoRu surfaces from first-principle density functional theoretical calculations. The reactions include CO activation, CH_x hydrogenation, CH_x coupling, water formation, in addition to the energetics associated with CO and H_2 adsorption and the desorption of water and the C_2H_x products that form. The results indicate that CO activation occurs at step edges or defect sites. This is consistent with experimental STM studies over ideal Co substrates performed by Shell Chemical Company. The subsequent hydrogenation steps and hydrocarbon coupling steps appear to be more favorable over the terrace sites on Co. While the activation barriers and the energetics indicate the terrace sites are more favorable for hydrocarbon coupling, it is not yet clear whether they actually control chain growth. This will depend upon the barriers for C and CH_x species that form at the step sites to diffuse out onto the terraces. If the intrinsic rate for diffusion away from the step edges is faster than that for hydrocarbon coupling at the step edge, the coupling reactions will occur out on the terraces. Otherwise the CH_x intermediates that form will recombine before they can escape out onto the terrace sites. The kinetic simulations indicate that the surface is predominantly covered in CO. The CH* species is the most predominant hydrocarbon intermediate on the surface. The carbon atoms that form readily hydrogenate to form CH*. The subsequent CHx* hydrogenation steps are slower. The formation of longer chain hydrocarbons is quite sensitive to the rates for hydrogenation verses CH coupling. The simulations reveal that there is an optimal balance between the kinetics of these two reactions which controls chain growth. The addition of Ru, helps to aid in the activation of CO and will likely help to enhance catalytic activity.

The product selectivities for FT are strongly influence by the metal. Moving toward the left in the transition metal series shuts down the activation of CO and enhances the production of methanol. Cu and Pd both appear to be fairly selective to methanol formation. Surface alloys of Sn in Pt(111) and pseudomorphic overlayers of Au/Cd(0001) also appear to be selective. As far as we can tell these two bimetallic systems have never been examined experimentally and may offer hope in enhancing CO to methanol. The results for the synthesis of ethanol are still very preliminary. We plan to extend the work in this area of oxygenate synthesis in future efforts.

VIII. REFERENCES

1. Geerlings, J.J.C., J.H. Wilson, G.J. Kramer, H.P.C.E. Kuipers, A. Hoek, and H.M. Huisman, *Fischer-Tropsch Technology - From Active Site to Commercial Process.* Appl. Catal. A, 1999. **186**: p. 27-40.
2. Ge, Q., M. Neurock, H.A. Wright, and N. Srinivasan, *A first principles study of carbon-carbon coupling over the {0001} surfaces of Co and Ru.* Journal of Physical Chemistry B, 2002. **106**(11): p. 2826-2829.
3. Ge, Q.F. and M. Neurock, *Adsorption and activation of CO over flat and stepped Co surfaces: A first principles analysis.* Journal of Physical Chemistry B, 2006. **110**(31): p. 15368-15380.
4. Fischer, F. and H. Tropsch, *Preparation of Synthetic Oil Mixtures (Synthol) From Carbon Monoxide and Hydrogen. I.* Brennstoff-Chem., 1923. **4**: p. 276-285.
5. Fischer, F. and H. Tropsch, *Preparation of Synthetic Oil (Synthol) From Carbon Monoxide and Hydrogen. II.* Brennstoff-Chem., 1924. **5**: p. 201-208.
6. Anderson, R.B., *The Fischer-Tropsch Synthesis*. 1984, New York: Academic Press.
7. Iglesia, E., S.C. Reyes, R.J. Madon, and S.L. Soled, *Selectivity Control and Catalyst Design in the Fischer-Tropsch Synthesis - Sites, Pellets, and Reactors.* Advances in Catalysis, 1993. **39**: p. 221-302.
8. Iglesia, E., *Design, Synthesis, and Use of Cobalt-based Fischer-Tropsch Synthesis Catalysts.* Applied Catalysis A, 1997. **161**(1-2): p. 59-78.
9. Thomas, J.M. and W.J. Thomas, *Principles and Practices of Heterogeneous Catalysis*. 1997, Weinheim: VCH Publishing Company.
10. van der Laan, G.P., A.A.C.M. Beenackers, and R. Krishna, *Multicomponent reaction engineering model for Fe-catalyzed Fischer-Tropsch synthesis in commercial scale slurry bubble column reactors.* Chemical Engineering Science, 1999. **54**(21): p. 5013-5019.
11. Dry, M.E., *The Fischer-Tropsch process: 1950-2000.* Catalysis Today, 2002. **71**(3-4): p. 227-241.
12. Vannice, M.A., J. Catal., 1975. **37**: p. 462.
13. Vannice, M.A., Catal. Rev. Sci. Eng., 1976. **14**: p. 153.
14. Vannice, M.A., *Catalysis: Science and Technology*. Vol. 3. 1982, Berlin: Springer-Verlag.
15. Biloen, P., J.N.Helle and W.H.M. Sachtler, J. Catal., 1979. **58**: p. 58.
16. Brady, R.C., and R. Pettit, J. Amer. Chem. Soc., 1980. **102**: p. 6181.
17. Brady, R.C.a.R.P., J. Am. Chem. Soc., 1981. **103**: p. 1287.
18. De Swart, J.W.A., R. Krishna, and S.T. Sie, *Selection, Design and Scale Up of the Fischer-Tropsch Reactor.* Stud. in Surf. Sci. and Catal., 1997. **107**: p. 213-218.
19. Espinoza, R.L., A.P. Steynberg, B. Jager, and A.C. Vosloo, *Low Temperature Fischer Tropsch Synthesis from a Sasol Perspective.* Appl. Catal A, 1999. **186**: p. 13-26.
20. Jager, B., *Developments in Fischer-Tropsch Technology*, in *Natural Gas Conversion*, R.L.E. M. de Pontes, C.P. Nicolaides, J.H. Scholz, and M.S. Scurrell, Editor. 1997, Elsevier Science, B.V.: Amsterdam.

21. Oukaci, R., A.H. Singleton, and J.G.Goodwin, *Comparision of Patented Co F-T Catalysts Using Fixed-Bed and Slurry Bubble Column Reactors.* Appl. Catal. A., 1999. **186**: p. 129-144.
22. Price, J.G., D.Glasser, D. Hildebrandt, and N.J. Coville, *Fischer-Tropsch Synthesis: DRIFTS and SIMS Surface Investigation of Co and Co/Ru onTitania Supports*, in *Natural Gas Conversion IV*, R.L.E. M. de Pontes, C.P. Nicolaides, J.H. Scholz and M.S. Scurrell, Editor. 1997, Elseier Science, B.V.: Amsterdam. p. 243-248.
23. Schulz, H., *Short History and Present Trends of Fischer-Tropsch Synthesis.* Appl. Catl. A, 1999. **186**: p. 3-12.
24. vanSanten, R.A. and M. Neurock, *Molecular Heterogeneous Catalysis: A Conceptual and Computational Approach*. 2006, Weinheim: Wiley-VCH.
25. Vansanten, R.A. and M. Neurock, *Concepts in Theoretical Heterogeneous Catalytic Reactivity.* Catalysis Reviews-Science and Engineering, 1995. **37**(4): p. 557-698.
26. Masel, R.I., *Principles of Adsorption and Reaction on Solid Surfaces*. 1996: Wiley.
27. Kresse, G. and J. Furthmuller, *Efficiency of ab-initio total energy calculations for metals and semiconductors using a plane-wave basis set.* Computational Materials Science, 1996. **6**(1): p. 15-50.
28. Kresse, G. and J. Furthmuller, *Efficient iterative schemes for ab initio total-energy calculations using a plane-wave basis set.* Physical Review B, 1996. **54**(16): p. 11169-11186.
29. Vanderbilt, D., *Soft Self-Consistent Pseudopotentials in a Generalized Eigenvalue Formalism.* Physical Review B, 1990. **41**(11): p. 7892-7895.
30. Perdew, J.P., J.A. Chevary, S.H. Vosko, K.A. Jackson, M.R. Pederson, D.J. Singh, and C. Fiolhais, *Atoms, Molecules, Solids, and Surfaces - Applications of the Generalized Gradient Approximation for Exchange and Correlation.* Physical Review B, 1992. **46**(11): p. 6671-6687.
31. Monkhorst, H.J. and J.D. Pack, *Special points for Brillouin-zone integrations.* Physical Review B, 1976. **13**(12-15): p. 5188-5192.
32. Henkelman, G., B. Uberuaga, and H. Jonsson, *A climbing image nudged elastic band method for finding saddle points and minimum energy paths.* J. Chem. Phys., 2000. **113**(22): p. 9901.
33. Henkelman, G. and H. Jonsson, *Improved tangent estimate in the nudged eleastic band method for finding minimum energy paths and saddle points.* J. Chem. Phys., 2000. **113**(22): p. 9978.
34. Neurock, M. and E.W. Hansen, *First-principles-based molecular simulation of heterogeneous catalytic surface chemistry.* Computers & Chemical Engineering, 1998. **22**: p. S1045-S1060.
35. Neurock, M., P.S. Venkataraman, and E.W. Hansen, *From first-principles quantum chemistry to catalytic kinetics.* Abstracts of Papers of the American Chemical Society, 1999. **217**: p. U654-U654.
36. Kieken, L., M. Neurock, and D. Mei, *First-Principles Based Kinetic Monte-Carlo Simulation of the Steady-State Decomposition of Nitric Oxide in Excess Dioxygen*

on Pt-Au(100) Alloy Model Surfaces. J. Phys. Chem. B, 2005. **109**(6): p. 2234-2244.
37. Mei, D., E.W. Hansen, and M. Neurock, *Ethylene Hydrogenation over Bimetallic Pd/Au(111) Surfaces: Application of Quantum Chemical Results and Dynamic Monte Carlo Simulation.* J. Phys. Chem. B, 2003. **107**(3): p. 798-810.
38. Mei, D., Q. Ge, M. Neurock, L. Kieken, and J. Lerou, *First-Principles-Based Dynamic Monte Carlo Simulation of Nitric Oxide Decomposition over Pt and Rh Surfaces under Lean-burn Conditions.* Mol. Physics, 2004. **102**(4): p. 361-369.
39. Hansen, E.W. and M. Neurock, *Modeling surface kinetics with first-principles-based molecular simulation.* Chemical Engineering Science, 1999. **54**(15-16): p. 3411-3421.
40. Hansen, E.W. and M. Neurock, *First-Principles-Based Simulation of Ethylene Hydrogenation Kinetics on Pd(100),.* J. Catal., 2001. **196**(2): p. 241-252.
41. Shustorovich, E., *Coverage Effects under Atomic Chemisorption - Morse-Potential Modeling Based on Bond-Order Conservation.* Surface Science, 1985. **163**(1): p. L645-L654.
42. Shustorovich, E., *Formation and Reaction of Allylic Species on Silver Surfaces - Bond-Order Conservation Morse-Potential Analysis.* Surface Science, 1992. **279**(3): p. 355-366.
43. Shustorovich, E. and A.T. Bell, *Analysis of Reaction Pathways Using the Bond-Order-Conservation Method.* Abstracts of Papers of the American Chemical Society, 1987. **194**: p. 206-COLL.
44. Sellers, H., *Relationship among Force-Constants Implied by the Principle of Bond-Order Conservation in Chemisorbed Systems.* Journal of Physical Chemistry, 1994. **98**(3): p. 968-971.
45. Sellers, H. and E. Shustorovich, *Chemistry of sulfur oxides on transition metal surfaces: A bond order conservation Morse potential modeling perspective,* in *11th International Congress on Catalysis - 40th Anniversary, Pts a and B.* 1996. p. 1243-1252.
46. Halgren, T.A., *Merck molecular force field .1. Basis, form, scope, parameterization, and performance of MMFF94.* Journal of Computational Chemistry, 1996. **17**(5-6): p. 490-519.
47. Halgren, T.A., *Merck molecular force field .2. MMFF94 van der Waals and electrostatic parameters for intermolecular interactions.* Journal of Computational Chemistry, 1996. **17**(5-6): p. 520-552.
48. Toomes, R.L. and D.A. King, *The adsorption of CO on Co{10(1)over-bar0}.* Surface Science, 1996. **349**(1): p. 1-18.
49. Gu, J., Y.Y. Yeo, W.S. Sim, and D.A. King, *Kinetic constraints in the phase transitions of chemisorbed carbon monoxide on Co{10(1)over-bar0} at high coverages.* Journal of Physical Chemistry B, 2000. **104**(19): p. 4684-4689.
50. Jenkins, S.J. and D.A. King, *Theory of CO adsorption on Co {10(1)over-bar0}.* Surface Science, 2002. **504**(1-3): p. 138-144.
51. Welz, M., W. Moritz, and D. Wolf, *Structure Determination of the Clean Co(1120) Surface by Leed.* Surface Science, 1983. **125**(2): p. 473-480.

52. Prior, K.A., E.G. Scott, and R.M. Lambert, *An X-Ray and Uv Photoelectron Spectroscopic Study of Co Chemisorption and Dissociation on the Stepped Co(1012) Surface.* Chemical Physics Letters, 1981. **80**(3): p. 517-520.
53. Venvik, H.J., C. Berg, and A. Borg, *CO adsorption on Co(10(1)over-bar-2) - a STM study.* Surface Science, 1998. **404**(1-3): p. 57-61.
54. Venvik, H.J., A. Borg, and C. Berg, *Formation of the GO-induced (3x1) surface structure on Co(11(2)over-bar0) studied by STM.* Surface Science, 1998. **397**(1-3): p. 322-332.
55. Papp, H., *Chemisorption and Reactivity of Carbon-Monoxide on a Co(112bar0) Single-Crystal Surface - Studied by Leed, Ups, Eels, Aes and Work Function Measurements.* Surface Science, 1985. **149**(2-3): p. 460-470.
56. Ponec, V., and W.A.A. van Barneveld, Ind. Eng. Chem. Res. Dev., 1979. **18**: p. 168.
57. Ponec, V.a.G.C.B., *Catalysis by Metals and Alloys*. 1995, Amsterdam: Elsevier.
58. Liu, X.M., G.Q. Lu, Z.F. Yan, and J. Beltramini, *Recent advances in catalysts for methanol synthesis via hydrogenation of CO and CO2.* Industrial & Engineering Chemistry Research, 2003. **42**(25): p. 6518-6530.
59. Krishnamoorthy, S., M. Tu, M.P. Ojeda, D. Pinna, and E. Iglesia, *An investigation of the effects of water on rate and selectivity for the Fischer-Tropsch synthesis on cobalt-based catalysts.* Journal of Catalysis, 2002. **211**(2): p. 422-433.
60. Ge, Q., S. Desai, M. Neurock, and K. Kourtakis, *CO adsorption on Pt-Ru surface alloys and on the surface of Pt-Ru bulk alloy.* Journal of Physical Chemistry B, 2001. **105**(39): p. 9533-9536.
61. Jerdev, D.I., R. Prins, and B.E. Koel, *Alloy formation and CO adsorption on bimetallic Ca/Pd(111) surfaces.* Journal of Physical Chemistry B, 2004. **108**(38): p. 14417-14427.
62. Burch, R. and M.J. Hayes, *The Preparation and Characterisation of Fe-Promoted Al2O3-Supported Rh Catalysts for Selective Production of Ethanol from Syngas,"*. J. Catal., 1997. **165**: p. 249-261.
63. Burch, R. and M.I. Petch, *Investigation of the Synthesis of Oxygenates from Carbon Monoxide/Hydrogen Mixtures on Supported Rhodium Catalysts.* Appl. Catal. A: Gen., 1992. **88**: p. 39-60.
64. Bowker, M., Catal. Today, 15, 77-100 (1992). *"On the Mechanism of Ethanol Synthesis on Rhodium"*. Catal. Today,, 1992. **15**: p. 77-100.
65. Matsuzaki, T., K.Takeuchi, T. Hanaoka, H. Arawaka, and Y. Sugi, *"Effect of Transition Metals on Oxygenates Formation from Syngas over Co/SiO2"*. Appl. Catal. A: Gen., 1993. **105**: p. 159-184.

IX. APPENDIES

Table A1. Adsorption energies and bond distances for optimized structure of methylidyne (CH) on Co$\{10\bar{1}2\}$ surface.

Adsorption site	Configuration	Adsorption energy (eV)	$d_{C\text{-}Co}$ (Å)	$d_{C\text{-}H}$ (Å)
Atop	A	-4.50	1.640	1.097
	C	-4.43	1.647	1.093
Bridge	B	-5.59	1.791, 1.809	1.099
	F	-5.49	1.800, 1.801	1.104
	G	-5.60	1.813, 1.804	1.096
3-fold hollow	H	-6.14	1.878, 1.925, 1.928	1.099
	I	-6.14	1.882, 1.901, 1.901	1.107
4-fold bridging	D	-6.35	1.885, 1.925,1.989, 1.989	1.105
4-fold hollow	J	-6.76	1.971, 1.976, 1.978, 1.978	1.114
	K	-6.75	1.973, 1.976, 1.978, 1.985	1.109

Table A2. Adsorption energies and bond distances for optimized structure of methylene (CH_2) on Co$\{10\bar{1}2\}$ surface.

Adsorption site	Configuration	Adsorption energy (eV)	$d_{C\text{-}Co}$ (Å)	$d_{C\text{-}H}$ (Å)
Atop	A	-2.91	1.771	1.098, 1.103
	A (twisted H's)	-3.16	1.766	1.094, 1.101
	C	-2.86	1.787	1.098, 1.099
	C (twisted H's)	-2.85	1.798	1.095, 1.101
Bridge	B	-3.57	1.937, 1.944	1.102, 1.103
	F	-3.85	1.925, 1.931	1.099, 1.099
	G	-3.58	1.944, 1.947	1.102, 1.103
3-fold hollow	H	-3.86	1.954, 2.125, 2.128	1.112, 1.124
	I	-3.88	1.963, 2.144, 2.156	1.118, 1.119
4-fold bridging	D'	-3.84	1.980, 2.137, 2.158	1.105, 1.127
	M	-3.90	1.952, 2.246, 2.293, 2.308, 2.354	1.117, 1.124
	M (twisted H's)	-3.26	1.9291, 2.239, 2.264, 2.271, 2.304	1.139, 1.142
4-fold hollow	J	-4.09	2.055, 2.056, 2.091, 2.098	1.125, 1.126
	K	-4.10	2.047, 2.063, 2.097, 2.114	1.119, 1.127

Table A3. The total energies for co-adsorbed methylidyne (CH) and methylene (CH_2) on Co$\{10\bar{1}2\}$ surface. The adsorption site for CH and CH_2 in the table reflect the sites where the C end groups of the CH_x intermediates adsorb on the surface.

Adsorption site CH	Adsorption site CH_2	Co-adsorbed energy (eV)
F	G	-145.04693
H	F	-146.08527
J	A	-146.74835
J	D’	-146.98161
J	M	-146.60248
J	I	-146.61584
D’	J	-146.59020

Table A4. Adsorption characterstics for vinyl(C_2H_3) adsorbed on Co$\{10\bar{1}2\}$ surface. The adsorption site for CH and CH_2 in the table reflect the sites where the C end groups of the C_2H_3 adsorb on the surface.

Adsorption site CH	Adsorption site CH_2	Adsorption Energy (eV)
A	F	-1.93
C	G	-1.65
F	G	-2.77
G	B	-2.71
G	F	-2.75
G	C	-2.64

Table A5. The total energies for co-adsorbed methylidyne (CH) and carbon (C) on $Co\{10\bar{1}2\}$ surface. The adsorption site for CH and C in the table reflect the sites where the C termini of the CH_x intermediates adsorb on the surface.

Adsorption site CH	Adsorption site C	E(eV)
M	J	-139.35339
J	M	-139.06994
J	D’	-139.55795

Table A6. Adsorption characteristics for C_2H adsorbed on Co$\{10\bar{1}2\}$ surface. The adsorption site for CH and C in the table reflect the sites where the C end groups of the C_2H adsorb on the surface.

Adsorption site CH	Adsorption site C	Adsorption Energy (eV)
F	J	-5.8
F	H	-5.58
G	J	-5.66
G	M	-5.17
G	I	-5.49
A	D’	-5.03
A		-3.86
B		-4.31
F		-4.40
G		-4.29